



CHORUS

This is the accepted manuscript made available via CHORUS. The article has been published as:

Treating different bonding situations: Revisiting Au-Cu alloys using the random phase approximation

Niraj K. Nepal, Santosh Adhikari, Jefferson E. Bates, and Adrienn Ruzsinszky

Phys. Rev. B **100**, 045135 — Published 25 July 2019

DOI: [10.1103/PhysRevB.100.045135](https://doi.org/10.1103/PhysRevB.100.045135)

Treating different bonding situations: Revisiting Au-Cu alloys using the random phase approximation

Niraj K. Nepal^{1,*}, Santosh Adhikari¹, Jefferson E. Bates², and Adrienn Ruzsinszky¹

[1] *Department of Physics, Temple University,
Philadelphia, Pennsylvania 19122, United States and*

[2] *A.R. Smith Department of Chemistry and Fermentation Sciences,
Appalachian State University, Boone, North Carolina 28607, United States*

(Dated: July 12, 2019)

Abstract

The ground state equilibrium properties of copper-gold alloys have been explored with the state-of-the-art random phase approximation (RPA). Our estimated lattice constants agree with the experiment within a mean absolute percentage error (MAPE) of 1.4 percent. Semi-local functionals such as the generalized gradient approximation (GGA) of Perdew, Burke, and Ernzerhof (PBE) and strongly constrained and appropriately normed (SCAN) fail to provide accurate bulk moduli, which indicate their inability to describe the system in a stretched or compressed state with respect to the equilibrium geometry. **The PBE, PBE revised for solids (PBESol), and revised TPSS (revTPSS) by Perdew et. al. predict too-low formation energies while the SCAN slightly overestimates it. The inclusion of thermal correction or the long-range dispersion provides negligible contribution to the formation energies estimated with semilocal density functional theory (DFT). The spin-orbit coupling (SOC) improves the formation energies of PBE only by 7-8 meV, while it intensifies the overestimation of SCAN.** We found that the non-locality present in RPA is able to describe the transition between two delocalized electron densities (bulk elemental constituents to crystallized alloys), as required to provide accurate formation energies **without any further corrections**. Based on our results, we conclude that it is difficult to find a universal density functional which can give accurate results for a wide range of properties of inter-metallic alloys. However, RPA can capture different bonding situations, often better than other density functionals. It gives accurate results for a wide range of ground state properties for the alloys, generated from metals with completely filled d-shells.

I. Introduction

Inter-metallic alloys, the mixture of 2 or more metals in a solid form, manifest a defined stoichiometry and an ordered crystal structure¹. The brittleness and high melting point with various electronic and magnetic properties of these solid compounds make them significantly useful in industrial applications. The heat of formation or formation energy of an alloy is the difference between the total binding energy of the system and its pure constituents, and its accurate prediction is extremely important in alloy theory. It governs the stability of the alloys with different compositions at different temperatures and pressures^{1,2}.

Density functional theory (DFT) is a robust electronic structure method, applicable across numerous fields of science. Various forms of the approximation to the exchange-correlation (XC-) energy, a key but unknown quantity in DFT, afford different levels of accuracy and computational efficiency. These different forms constitute the different rungs of Perdew's Jacob's ladder³. The local density approximation (LDA)⁴ and generalized gradient approximations (GGA) such as PBE⁵, AM05 by Armiento and Mattsson⁶, and PBE revised for solids (PBESol)⁷, though being highly accurate and efficient in many cases, often fail to provide an accurate description of the properties which require either self-interaction correction, at least a fraction of exact exchange, or an adequate description of many-body correlation⁸. Meta-GGAs such as TPSS⁹ by Tao, Perdew, Staroverov, and Scuseria, the made-simple (MS) family^{10,11}, and

SCAN¹² provide significant improvement over LDA and GGAs, with the inclusion of kinetic energy density ($\tau(\mathbf{r})$) as an ingredient in addition to the density ($n(\mathbf{r})$) and its gradient ($\nabla n(\mathbf{r})$). However, regarding the formation energy of inter-metallic alloys, semi-local functionals have a mixed performance¹³⁻¹⁵. To estimate an accurate formation energy, a functional should not only provide reliable energetics of an alloy but also simultaneously of its constituent elements. However, most semi-local functionals fail in that regard, leading to inaccurate predictions of the formation energy¹⁶.

At high temperature, copper and gold form a continuous solid solution while they crystallize to form Au-Cu super-lattices at lower temperature¹⁷. The Au-Cu systems, AuCu₃ (or Au_{0.25}Cu_{0.75}), AuCu (or Au_{0.5}Cu_{0.5}), and CuAu₃ (or Au_{0.75}Cu_{0.25}), are the paradigms of inter-metallic alloys, and have been extensively studied with semi-local as well as non-local DFT methods¹⁴⁻¹⁶. Experimentally, the fully ordered AuCu₃ and CuAu₃ stabilize in the L1₂ phase while the ordered AuCu prefers the L1₀ phase at T = 0 K¹. In addition to the distorted face-centered cubic (FCC) phase for AuCu (L1₀), we also have explored its FCC phase. Previous work clearly established that LDA could not predict the ground state of CuAu₃ as the L1₂ phase and also significantly underestimates the formation energies of all the Au-Cu alloys¹⁵. Similar to LDA, PBE also predicts CuAu₂ as the stable phase and CuAu₃ as the unstable one¹⁴. On the other hand, the screened hybrid XC-functional HSE06 (simply HSE by Heyd, Scuseria, and Ernzerhof)^{18,19} developed by mixing non-local exact

exchange with semi-local exchange-correlation, is able to provide accurate geometries and formation energies of these compounds¹⁴. Moreover, HSE is designed to be nonlocal at short range, while the exact exchange is screened at long range. SCAN was demonstrated to capture medium-range weak interactions, while HSE is known to reduce the delocalization error in semilocal functionals. Inspired by these facts, we aim to climb even higher on the rungs of Jacob’s ladder to gain more understanding about any competition between weak interactions and free electron-like bonding in Cu-Au systems²⁰.

In this work, we have revisited the Au-Cu alloy systems using the random phase approximation (RPA)^{21–23}. RPA is the simplest approximation within an adiabatic-connection fluctuation-dissipation theorem (ACFDT) formalism^{24,25}. It combines the non-local one electron self-interaction free exact exchange (EXX) energy with the non-local correlation energy (E_C^{RPA})^{26,27}. Most importantly, it can provide accurate results for systems involving weak interactions such as van der Waals (vdW) interactions^{28–30}, as well as ionic^{20,31} and covalent interactions^{20,32–34}. The total energy in the ACFDT-DFT framework can be expressed as,

$$E = E_{EXX} + E_C^{RPA} \quad (1)$$

where, E_{EXX} is the Hartree-Fock (HF) total energy evaluated non-self-consistently using self-consistently-obtained Kohn-Sham DFT orbitals. E_C^{RPA} is the RPA correlation energy, which can be obtained using the interacting density-density response function (χ) which is related to the non-interacting response function (χ_0) via a Dyson-like equation^{26,27,35}. The RPA correlation energy naturally incorporates long-range dispersion and is non-perturbative. For this work, the systems are heavy coinage metals which are largely influenced by dispersion interactions^{36–38}. Furthermore, the systems have zero band gap. Due to its non-perturbative nature, RPA can be safely applied to zero-gap systems without divergence³⁹. In both aspects, the application of RPA to these systems is justified.

For the sake of comparison, we also have assessed semi-local functionals such as PBE, PBEsol, the revised TPSS (revTPSS)^{40,41} and SCAN along with RPA. **We also tested the impact of long-range dispersion through the nonlocal revised VV10 (rVV10) correction. We utilized PBE+rVV10^{42,43} and SCAN+rVV10⁴⁴ to check whether the discrepancies in semilocal DFT are due to the absence of long-range dispersion interactions.** The rest of the paper is organized as follows. Computational details are provided in section II, followed by results in section III. We will present our conclusions in section IV.

II. Computational details

All DFT calculations were carried out using a **projector augmented wave (PAW)**⁴⁵ method, as implemented in GPAW^{46–48} and VASP⁴⁹. We utilized VASP to perform semi-local calculations whereas RPA calculations were carried out using GPAW. Moreover, semi-local calculations were performed self-consistently while RPA calculations were carried out using a non-self-consistent approach. We used a plane-wave cutoff of 600 eV and Brillouin zone sampling of $20 \times 20 \times 20$ Gamma centered k-mesh to avoid the convergence test for semi-local DFT calculations. Ground state PBE calculations were performed as an input for the RPA calculations. Separate convergence tests for EXX and the RPA correlation energies were carried out to determine the plane-wave cutoffs and k-mesh sampling with less than 2 meV relative error (**Supplementary Table S1**⁵⁰). We used a maximum cutoff of 350 eV to compute the response function. All other parameters and procedure of the RPA calculations were kept similar to that of Ref. 31, except skipping the gamma point ($\mathbf{q} = 0$) to avoid the possible divergent contribution from metals as discussed in Ref. 32.

We calculated the zero-point vibrational energy (ZPVE) to estimate the thermal contribution to the formation energy. PBEsol⁷ calculations were done with a $2 \times 2 \times 2$ supercell (32 atoms) using VASP^{51,52} and PHONOPY⁵³. The estimated thermal corrections are less than or equal to 1 meV/atom, consistent with previous results¹⁴. Relativistic effects are included at the scalar level for each atom within the PAW potentials provided in VASP and GPAW. **We further tested, at least for PBE and SCAN, an impact of the spin-orbit coupling⁵⁴ on semi-local DFT results.** We have performed calculations for 7 volume points near the experimental equilibrium volume and fit the Birch-Murnaghan equation of state⁵⁵ to evaluate the equilibrium properties. We have used the experimental structures from Ref. 17 and varied the lattice constants isotropically to generate structures with different volumes. In order to compute the cohesive energies, atomic energies were computed. We have performed spin polarized semi-local DFT calculations with VASP using a plane-wave cutoff of 600 eV and $23 \times 24 \times 25 \text{ \AA}^3$ simulation cell to avoid any interactions of an isolated atom with its periodic images. Separate convergence tests for atomic energies were performed with GPAW for both EXX and RPA (**Supplementary Table S1**⁵⁰).

III. Results

A. Lattice constants

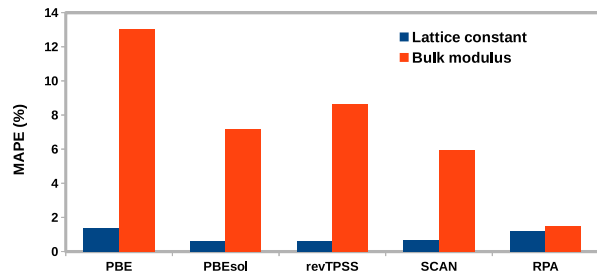
The equilibrium lattice constants of the ordered Au-Cu alloys are presented in Table I. As expected, PBE overestimates the lattice constants and PBEsol yields reasonable lattice constants of the coinage metals such as

Au and Cu²⁰. The failure of PBE to estimate accurate lattice constants is related to the poor descriptions of **exchange-correlation** effects between completely filled d-shells in coinage metals²⁰. RPA lattice constants are also overestimated which can be decreased by including the Pauli repulsion in SOSEX or adding a kernel correction to RPA^{31,56,57}, thereby improving the short-range correlations necessary to describe the systems with more filled d-shells. On the other hand, SCAN along with revTPSS show good performance in the prediction of equilibrium lattice constant. With the inclusion of kinetic energy density, both SCAN and revTPSS can distinguish different bonding regions relevant to lattice constants, and this becomes more effective as more d bands are filled in the transition metal²⁰. Overall, all methods show a reasonable agreement with the experiment for the lattice constant with mean absolute percentage error (MAPE) less than 1.4%, as shown in Figure 1. **Furthermore, the addition of long-range dispersion correction slightly improves the PBE lattice constants, while it slightly worsens the SCAN results (Supplementary Table S2⁵⁰). The inclusion of spin-orbit coupling can change the PBE and SCAN lattice constants by 1 picometer (Supplementary Table S3⁵⁰).**

TABLE I. Lattice constants (Å). The experimental lattice constants are taken from Reference 17. Among the DFT functionals utilized, PBEsol shows the best performance in predicting the equilibrium lattice constant.

	PBE	PBEsol	revTPSS	SCAN	RPA	Experiment
Cu	3.64	3.57	3.57	3.57	3.63	3.62
Au	4.16	4.08	4.08	4.09	4.15	4.08
AuCu ₃	3.78	3.72	3.72	3.72	3.78	3.75
AuCu (FCC)	3.92	3.85	3.85	3.85	3.92	3.87
AuCu (P4/mmm)	2.84	2.79	2.79	2.79	2.83	2.80
CuAu ₃	4.05	3.97	3.98	3.98	4.05	3.95
MAE (Å)	0.051	0.022	0.023	0.026	0.046	-
MAPE (%)	1.37	0.59	0.64	0.7	1.21	-

FIG. 1. **Mean absolute percentage error (MAPE) for both lattice constants and the bulk moduli. Overall, PBEsol is the most accurate method for lattice constants, while RPA predicts excellent bulk moduli compared to experiments.**



B. Bulk Moduli

The bulk modulus measures the curvature of an energy-volume relation, and its accurate prediction indicates the ability of a DFT approximation to describe the system in a non-equilibrium state with respect to the equilibrium state. We calculated the bulk moduli of various Au-Cu systems and tabulated them in Table II. PBE underestimates the bulk modulus, while PBEsol and revTPSS predict accurate bulk moduli for gold. However, the performance of these functionals worsens on increasing the concentration of copper. On the other hand, SCAN provides an improvement for the bulk modulus of copper, thereby improving the bulk moduli of all alloys compared to PBEsol and revTPSS (Figure 1). The inability of semi-local functionals to give an accurate prediction of bulk moduli indicates their inability to describe the compressed or stretched electron densities with respect to the equilibrium ground state electron densities. One can see that the overall bulk moduli predicted by PBE for all the alloys are close to the experimental value of copper while those of other semi-local functionals are closer to gold. On the other hand, RPA provides accurate bulk moduli for both alloys and those of the constituent bulk elemental systems. This indicates that, contrary to the lattice constant, the description of short-range correlation is not crucial for the prediction of the bulk modulus. **The inclusion of long-range dispersion via rVV10 provides a more significant correction to the bulk modulus for PBE than that for SCAN. On the other hand, spin-orbit coupling can increase the bulk moduli by 3-6 GPa with respect to DFT results without SOC (Supplementary Table S3⁵⁰).**

TABLE II. Bulk Modulus (GPa). Experimental bulk moduli are computed using $\frac{C_{11}+2C_{12}}{3}$ (cubic lattice), where C_{ij} is the elastic moduli. Overall, RPA predicts the bulk moduli in close agreement with the experiment.

	PBE	PBEsol	revTPSS	SCAN	HSE ⁵⁸	RPA	Experiment
Cu	137.89	164.50	170.14	157.91	133.8	144.74	143.6 ⁵⁹
Au	139.03	174.34	176.01	166.95	146.6	176.71	177.6 ⁶⁰ , 180.53 ⁵⁹
AuCu ₃	139.49	168.05	171.09	164.84	-	155.25	151.83 ⁶¹
AuCu (FCC)	139.99	171.02	173.12	169.47	-	163.77	162.97 ⁶²
AuCu (P4/mmm)	138.75	169.56	171.90	166.16	-	159.09	-
CuAu ₃	139.03	171.64	173.25	165.74	-	162.15	166.33 ⁶³
MAE (GPa)	21.71	11.04	13.19	9.31	-	2.42	-
MAPE (%)	13.02	7.20	8.65	5.93	-	1.50	-

C. Formation Energy

The formation energy of a Au-Cu alloy can be obtained using,

$$\Delta E_f(\text{Au}_x\text{Cu}_{1-x}) = \Delta E_{\text{coh}}(\text{Au}_x\text{Cu}_{1-x}) - x\Delta E_{\text{coh}}(\text{Au}) - (1-x)\Delta E_{\text{coh}}(\text{Cu}) \quad (2)$$

where $\Delta E_f(\text{Au}_x\text{Cu}_{1-x})$, $\Delta E_{\text{coh}}(\text{Au}_x\text{Cu}_{1-x})$, $\Delta E_{\text{coh}}(\text{Au})$, and $\Delta E_{\text{coh}}(\text{Cu})$ are the formation energy of the system, cohesive energy of the whole system, cohesive energy of gold, and the cohesive energy of copper per atom

respectively and x is the fraction of gold atoms in the alloys. We have computed the formation energy of a given alloy as a function of crystal volume, Figure 2. Experimental volumes are indicated by a ‘#’, whereas the formation energies are represented by black dots. Positive formation energies imply instability of the alloy while negative formation energies imply stability with respect to their elemental bulk constituents.

Without any correlation, EXX predicts destabilized systems within the range of volumes considered. Contrary to EXX, PBE stabilizes the systems with the presence of both exchange and correlation energies (Figure 2). Formation energies obtained from PBE agree with RPA values either at the highly compressed state or at the highly stretched state. However, they start to deviate from RPA and even from the experimental value as the equilibrium geometry is approached. On the contrary, SCAN slightly overbinds the formation energies near the equilibrium geometries, and the overestimation gets larger as we deviate from the equilibrium. The formation energy vs volume calculated with PBEsol and revTPSS behave similarly to that of SCAN, however, they are slightly shifted upward along the direction of positive formation energy. Despite the fact that RPA overestimates the lattice constant, it accurately predicts the curvature and minima of the equation of state for these alloys.

The heats of formation of the Au-Cu system at equilibrium are presented in Table III, whereas the stability of the alloys are represented by a convex hull as in Figure 3. As in the earlier studies^{14,16}, PBE severely underestimates the formation energies. On restoring the second-order gradient expansion for the exchange over a wide range of densities at the GGA level, PBEsol slightly improves the results, but at the meta-GGA level revTPSS⁶⁴ worsens it. By satisfying more exact constraints and including more appropriate norms¹², SCAN shows a considerable improvement over revTPSS. However, it still performs poorly for copper-rich alloys, while the error decreases on increasing the concentration of gold, as more filled 5d shells in Au are involved²⁰. **The deficiencies in semi-local PBE and SCAN could not be overcome simply by taking thermal correction, long-range dispersion correction, or spin-orbit coupling into account (Supplementary Tables S2 and S3⁵⁰).** In contrast, non-local density functionals such as hybrid HSE and RPA consistently predict accurate formation energies of these alloys **without any aforementioned corrections**. In comparison, self-consistent HSE outperforms non-self-consistent RPA by only a little, but there can be room for improvement when RPA is also evaluated self-consistently⁶⁵.

In the present work, both alloys and the constituent metals are in the solid phase and hence possess delocalized electron densities. The reliable prediction of formation

energies requires an accurate description of the transition from delocalized electron densities of constituent metals to delocalized electron densities of inter-metallic alloys. All semi-local functionals included herein fail to describe such a transition, while the non-locality present in HSE and RPA is able to effectively detect such changes. However, the transition from localized (atoms) to delocalized (solid metals and alloys) is not straightforward even for non-local functionals, as evident from the cohesive energies presented in Table IV. The best density functional for formation energies is the worst for cohesive energies. The hybrid HSE seriously underestimates the cohesive energies of Au-Cu system with a mean absolute error (MAE) of nearly 0.7 eV/atom. Surprisingly, semi-local functionals perform much better than HSE in the order of PBE < revTPSS < PBEsol < SCAN with decreasing MAE and MAPE. RPA, on the other hand, provides reasonable cohesive energies for Cu-rich compounds, while it worsens on increasing the concentration of gold in the alloys. As the number of filled d bands increases, the short-range correlation becomes more crucial in describing the interactions within transition metal atoms as well as their alloys. Restoring the exchange-correlation kernel within the RPA can improve the cohesive energies of transition metals up to 0.3 to 0.4 eV^{34,66}.

The performance of various density functionals on Au-Cu alloys clearly depends on their ability to describe the less-delocalized “3d” electron density of copper as well as the more-delocalized “5d” electron density of gold. SCAN along with PBEsol and revTPSS can effectively describe the 5d bands of gold, thereby giving sensibly accurate lattice constants, bulk moduli, and cohesive energies for Au-rich alloys. However, RPA has the opposite trend that it can provide an accurate prediction for Cu-rich alloys, but falls short when describing Au-rich alloys. On the contrary, HSE fails to provide accurate bulk moduli and cohesive energies for both copper and gold, giving too low cohesive energies for both Au- and Cu- rich alloys. With that in mind, one can argue that the density functionals that can separately describe the constituents, can ultimately describe the weakly bonded alloys.

TABLE III. The heat of formation (eV /atom). Note that the results for semi-local functionals and HSE are obtained self-consistently, while the RPA results are obtained non-self-consistently using PBE orbitals. Experimental results taken from Reference 1 are obtained at 320 K, whereas Reference 2 corresponds to 298.15 K; CuAu₃: The experimental structure taken in Reference 1 is not fully ordered structure. The heat of formation for a fully ordered CuAu₃ is estimated using cubic interpolation of composition (x)-Gibbs energy (ΔG)-entropy (ΔS) of formation data taken from Reference 2.

	PBE	PBEsol	revTPSS	SCAN	HSE ¹⁴	RPA	Experiment ¹
AuCu ₃	-0.046	-0.050	-0.040	-0.093	-0.071	-0.080	-0.074, -0.075 ²
AuCu (FCC)	-0.047	-0.050	-0.037	-0.101		-0.088	
AuCu (P4/mmm)	-0.058	-0.062	-0.051	-0.111	-0.091	-0.096	-0.093
CuAu ₃	-0.026	-0.028	-0.019	-0.059	-0.053	-0.052	-0.039, -0.056 ²

TABLE IV. Cohesive energy per atom (eV/atom). The cohesive energies for HSE are obtained using References 14 and 58, while the experimental cohesive energies are obtained using References 1 and 67 using Eq. 2. Among the functionals used, SCAN predicts most accurate cohesive energy as compared to the experiment.

	PBE	PBEsol	revTPSS	SCAN	HSE	RPA	Experiment
Cu	3.484	4.030	4.057	3.886	3.060 ⁵⁸	3.350	3.490 ⁶⁷
Au	3.035	3.720	3.627	3.555	2.880 ⁵⁸	3.395	3.810 ⁶⁷
AuCu3	3.419	4.003	3.990	3.896	3.086	3.441	3.644
AuCu (P4/mmm)	3.317	3.937	3.893	3.828	3.111	3.469	3.743
CuAu3	3.175	3.826	3.753	3.695	2.978	3.436	3.786
MAE (eV/atom)	0.409	0.245	0.256	0.216	0.672	0.276	–
MAPE (%)	10.84	6.78	7.08	5.93	18.05	7.41	–

IV. Conclusions

We have explored copper-gold alloys with various levels of approximations within density functional theory, including the state-of-art random phase approximation. It is difficult to find a universal functional which can describe all of the bonding situations. Semi-local functionals can reasonably describe the transition between localized and delocalized electron densities, as manifested in the cohesive energies. On the other hand, the non-locality present in HSE and RPA can distinguish the transition between two delocalized electron densities, as seen from the formation energies of the alloys. Moreover, the performance of

these functionals in describing the weakly bonded Au-Cu system depends on their potential to separately describe less-delocalized and more-delocalized electron densities of copper and gold respectively. Based on our results, we can conclude that RPA predicts accurate values for diverse properties of binary alloys, generated from metals with completely filled d-shells. It has an accuracy of semi-local functionals at the challenging situations, while consistently providing reliable results where semi-local functionals break down.

V. Acknowledgements

N.K.N. and A.R. acknowledge support by the National Science Foundation under Grant No. DMR-1553022. JEB was supported by the A.R. Smith Department of Chemistry and Fermentation Sciences. Computational support was provided by Temple University’s HPC resources and thus was supported in part by the National Science Foundation through major research instrumentation grant number 1625061 and by the US Army Research Laboratory under contract number W911NF-16-2-0189. N.K.N., JEB, and A.R. designed the project. N.K.N. performed the calculations, and wrote the first draft. S.A. performed some of the calculations. All authors contributed references, discussions, and revisions.

* niraj.nepal@temple.edu

¹ R. Orr, *Acta Metall.* **8**, 489 (1960).

² R. Hultgren, P. D. Desai, D. T. Hawkins, M. Gleiser, and K. K. Kelley, *Selected values of the thermodynamic properties of binary alloys*, Tech. Rep. (National Standard Reference Data System, 1973).

³ J. P. Perdew and K. Schmidt, in *Density Functional Theory and Its Applications to Materials*, Vol. 577, edited by V. Van Doren, C. Van Alsenoy, and P. Geerlings (AIP Conference Proceedings, Melville, N.Y., 2001) pp. 1–20.

⁴ W. Kohn and L. J. Sham, *Phys. Rev.* **140**, A1133 (1965).

⁵ J. P. Perdew, K. Burke, and M. Ernzerhof, *Phys. Rev. Lett.* **77**, 3865 (1996).

⁶ R. Armiento and A. E. Mattsson, *Phys. Rev. B* **72**, 085108 (2005).

⁷ J. P. Perdew, A. Ruzsinszky, G. I. Csonka, O. A. Vydrov, G. E. Scuseria, L. A. Constantin, X. Zhou, and K. Burke, *Phys. Rev. Lett.* **100**, 136406 (2008).

⁸ P. Ziesche, S. Kurth, and J. P. Perdew, *Comput. Mater. Sci.* **11**, 122 (1998).

⁹ J. Tao, J. P. Perdew, V. N. Staroverov, and G. E. Scuseria, *Phys. Rev. Lett.* **91**, 146401 (2003).

¹⁰ J. Sun, B. Xiao, and A. Ruzsinszky, *J. Chem. Phys.* **137**, 051101 (2012).

¹¹ J. Sun, R. Haunschild, B. Xiao, I. W. Bulik, G. E. Scuseria, and J. P. Perdew, *J. Chem. Phys.* **138**, 044113 (2013).

¹² J. Sun, A. Ruzsinszky, and J. P. Perdew, *Phys. Rev. Lett.* **115**, 036402 (2015).

¹³ E. B. Isaacs and C. Wolverton, *Phys. Rev. Mater.* **2**, 063801 (2018).

¹⁴ Y. Zhang, G. Kresse, and C. Wolverton, *Phys. Rev. Lett.* **112**, 075502 (2014).

¹⁵ V. Ozoliņš, C. Wolverton, and A. Zunger, *Phys. Rev. B* **57**, 6427 (1998).

¹⁶ L.-Y. Tian, H. Levämäki, M. Ropo, K. Kokko, Á. Nagy, and L. Vitos, *Phys. Rev. Lett.* **117**, 066401 (2016).

¹⁷ H. Okamoto, D. J. Chakrabarti, D. E. Laughlin, and T. B. Massalski, *Journal of Phase Equilibria* **8**, 454 (1987).

¹⁸ J. Heyd, G. E. Scuseria, and M. Ernzerhof, *J. chem. phys.* **118**, 8207 (2003).

¹⁹ J. Heyd, G. E. Scuseria, and M. Ernzerhof, *The Journal of Chemical Physics* **124**, 219906 (2006).

²⁰ L. Schimka, R. Gaudoin, J. Klimeš, M. Marsman, and G. Kresse, *Phys. Rev. B* **87**, 214102 (2013).

²¹ D. Bohm and D. Pines, *Phys. Rev.* **85**, 338 (1952).

²² D. Bohm and D. Pines, *Phys. Rev.* **92**, 609 (1953).

²³ D. C. Langreth and J. P. Perdew, *Phys. Rev. B* **21**, 5469 (1980).

²⁴ D. C. Langreth and J. P. Perdew, *Solid State Commun.* **17**, 1425 (1975).

²⁵ D. C. Langreth and J. P. Perdew, *Phys. Rev. B* **15**, 2884 (1977).

²⁶ H. Eshuis, J. E. Bates, and F. Furche, *Theor. Chem. Acc.* **131**, 1084 (2012).

²⁷ X. Ren, P. Rinke, C. Joas, and M. Scheffler, *J. Mater. Sci.* **47**, 7447 (2012).

²⁸ J. Harl and G. Kresse, *Phys. Rev. B* **77**, 045136 (2008).

²⁹ L. Schimka, J. Harl, A. Stroppa, A. Grüneis, M. Marsman, F. Mittendorfer, and G. Kresse, *Nat. Mater.* **9**, 741 (2010).

- ³⁰ S. Lebègue, J. Harl, T. Gould, J. G. Ángyán, G. Kresse, and J. F. Dobson, *Phys. Rev. Lett.* **105**, 196401 (2010).
- ³¹ N. K. Nepal, A. Ruzsinszky, and J. E. Bates, *Phys. Rev. B* **97**, 115140 (2018).
- ³² J. Harl, L. Schimka, and G. Kresse, *Phys. Rev. B* **81**, 115126 (2010).
- ³³ H. Peng and S. Lany, *Phys. Rev. B* **87**, 174113 (2013).
- ³⁴ T. Olsen and K. S. Thygesen, *Phys. Rev. B* **87**, 075111 (2013).
- ³⁵ F. Furche, *Phys. Rev. B* **64**, 195120 (2001).
- ³⁶ C. L. Bracey, P. R. Ellis, and G. J. Hutchings, *Chemical Society Reviews* **38**, 2231 (2009).
- ³⁷ J. Mahanty and R. Taylor, *Phys. Rev. B* **17**, 554 (1978).
- ³⁸ A. L. Fetter and J. D. Walecka, *Quantum theory of many-particle systems* (Courier Corporation, 2012).
- ³⁹ N. Colonna, M. Hellgren, and S. de Gironcoli, *Phys. Rev. B* **90**, 125150 (2014).
- ⁴⁰ J. P. Perdew, A. Ruzsinszky, G. I. Csonka, L. A. Constantin, and J. Sun, *Phys. Rev. Lett.* **103**, 026403 (2009).
- ⁴¹ J. Sun, M. Marsman, G. I. Csonka, A. Ruzsinszky, P. Hao, Y.-S. Kim, G. Kresse, and J. P. Perdew, *Phys. Rev. B* **84**, 035117 (2011).
- ⁴² H. Peng and J. P. Perdew, *Phys. Rev. B* **95**, 081105(R) (2017).
- ⁴³ S. Adhikari, H. Tang, B. Neupane, G. I. Csonka, and A. Ruzsinszky, arXiv preprint arXiv:1906.01091 (2019).
- ⁴⁴ H. Peng, Z.-H. Yang, J. P. Perdew, and J. Sun, *Phys. Rev. X* **6**, 041005 (2016).
- ⁴⁵ P. E. Blöchl, *Phys. Rev. B* **50**, 17953 (1994).
- ⁴⁶ M. Walter, H. Häkkinen, L. Lehtovaara, M. Puska, J. Enkovaara, C. Rostgaard, and J. J. Mortensen, *J. Chem. Phys.* **128**, 244101 (2008).
- ⁴⁷ J. J. Mortensen, L. B. Hansen, and K. W. Jacobsen, *Phys. Rev. B* **71**, 035109 (2005).
- ⁴⁸ S. R. Bahn and K. W. Jacobsen, *Comput. Sci. Eng.* **4**, 56 (2002).
- ⁴⁹ J. Hafner, *J. Comput. Chem.* **29**, 2044 (2008).
- ⁵⁰ See Supplemental Material at [URL will be inserted by publisher] for files containing energy-volume data, a python script, and a pdf having information about the data, convergence tests referenced in the manuscript.
- ⁵¹ G. Kresse and J. Furthmüller, *Phys. Rev. B* **54**, 11169 (1996).
- ⁵² G. Kresse and D. Joubert, *Phys. Rev. B* **59**, 1758 (1999).
- ⁵³ A. Togo and I. Tanaka, *Scr. Mater.* **108**, 1 (2015).
- ⁵⁴ S. Steiner, S. Khmelevskiy, M. Marsmann, and G. Kresse, *Phys. Rev. B* **93**, 224425 (2016).
- ⁵⁵ F. Birch, *Phys. Rev.* **71**, 809 (1947).
- ⁵⁶ J. E. Bates, S. Laricchia, and A. Ruzsinszky, *Phys. Rev. B* **93**, 045119 (2016).
- ⁵⁷ A. Grüneis, M. Marsman, J. Harl, L. Schimka, and G. Kresse, *The Journal of chemical physics* **131**, 154115 (2009).
- ⁵⁸ P. Janthon, S. Luo, S. M. Kozlov, F. Vines, J. Limtrakul, D. G. Truhlar, and F. Illas, *Journal of chemical theory and computation* **10**, 3832 (2014).
- ⁵⁹ H. B. Huntington, *Solid state physics*, Vol. 7 (Elsevier, 1958) pp. 213–351.
- ⁶⁰ F. Cardarelli, *Materials Handbook: A Concise Desktop Reference* (Springer International Publishing, Cham, 2018) pp. 317–695.
- ⁶¹ S. G. O’Hara and B. J. Marshall, *Phys. Rev. B* **3**, 4002 (1971).
- ⁶² C. Teodosiu, *Elastic models of crystal defects* (Springer Science & Business Media, 2013).
- ⁶³ G. Simmons, *Single crystal elastic constants and calculated aggregate properties*, Tech. Rep. (SOUTHERN METHODIST UNIV DALLAS TEX, 1965).
- ⁶⁴ J. P. Perdew, A. Ruzsinszky, G. I. Csonka, L. A. Constantin, and J. Sun, *Physical Review Letters* **103**, 026403 (2009).
- ⁶⁵ N. L. Nguyen, N. Colonna, and S. de Gironcoli, *Phys. Rev. B* **90**, 045138 (2014).
- ⁶⁶ T. S. Jauho, T. Olsen, T. Bligaard, and K. S. Thygesen, *Phys. Rev. B* **92**, 115140 (2015).
- ⁶⁷ C. Kittel, P. McEuen, and P. McEuen, *Introduction to solid state physics*, Vol. 8 (Wiley New York, 1976).

FIG. 2. Formation energy (eV) versus volume (\AA^3). The positive formation energy refers to instability of alloys with respect to isolated bulk constituents, while negative formation energy refers to stability. Experimental formation energies are taken from References 1 and 2. The experimental volumes are indicated by '#' in Figures.

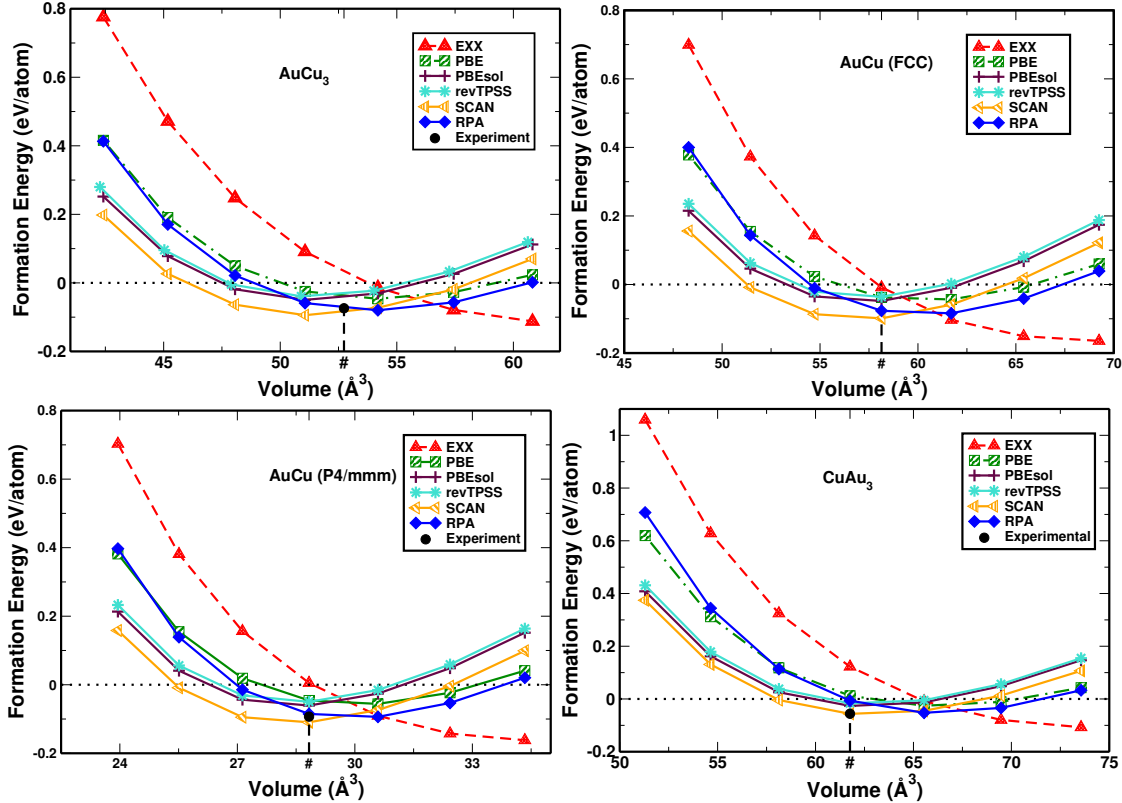


FIG. 3. Convex hull: Formation energy as a function of gold composition (x). PBE along with PBEsol and revTPSS largely underestimates the formation energy, while SCAN performs poorly on Cu-rich alloy, but improves the result as the concentration of gold increases. Formation energies predicted by non-local HSE and RPA are in close agreement with the experiment.

